frontiers in Materials

ORIGINAL RESEARCH
published: 10 March 2020
doi: 10.3389/fmats.2020.00049

Hierarchical HRP-Crosslinked Silk Fibroin/ZnSr-TCP Scaffolds for Osteochondral Tissue Regeneration: Assessment of the Mechanical and Antibacterial Properties

Viviana P. Ribeiro[1,2†], Sandra Pina[1,2*†], Sabina Gheduzzi[3], Ana C. Araújo[1,2], Rui L. Reis[1,2,4] and Joaquim M. Oliveira[1,2,4]*

[1] 3B's Research Group, Research Institute on Biomaterials, Biodegradables and Biomimetics, Headquarters of the European Institute of Excellence on Tissue Engineering and Regenerative Medicine, University of Minho, Guimarães, Portugal, [2] ICVS/3B's – PT Government Associate Laboratory, Braga/Guimarães, Portugal, [3] Centre for Orthopaedic Biomechanics, Department of Mechanical Engineering, University of Bath, Bath, United Kingdom, [4] The Discoveries Centre for Regenerative and Precision Medicine, Headquarters at University of Minho, Guimarães, Portugal

OPEN ACCESS

Edited by:
Antonella Motta,
University of Trento, Italy

Reviewed by:
Francesco Grassi,
Rizzoli Orthopedic Institute (IRCCS), Italy
José Pérez-Rigueiro,
Polytechnic University of Madrid, Spain

***Correspondence:**
Viviana P. Ribeiro
viviana.ribeiro@i3bs.uminho.pt
Sandra Pina
sandra.pina@i3bs.uminho.pt

[†] These authors have contributed equally to this work

Specialty section:
This article was submitted to Mechanics of Materials, a section of the journal Frontiers in Materials

Received: 23 October 2019
Accepted: 18 February 2020
Published: 10 March 2020

Citation:
Ribeiro VP, Pina S, Gheduzzi S, Araújo AC, Reis RL and Oliveira JM (2020) Hierarchical HRP-Crosslinked Silk Fibroin/ZnSr-TCP Scaffolds for Osteochondral Tissue Regeneration: Assessment of the Mechanical and Antibacterial Properties. Front. Mater. 7:49. doi: 10.3389/fmats.2020.00049

The biomaterials requirements for osteochondral (OC) defects restoration simultaneously include adequate mechanical behavior, and the prevention of bacterial adherence and biofilm formation, without impairing local tissue integration. Bilayered and hierarchical scaffolds combining a cartilage-like layer interconnected to an underlying subchondral bone-like layer appeared as innovative technological solutions able to mimic the native OC tissue hierarchical architecture. This study is focused on the assessment of the combined compression-shear stresses and possible bacterial biofilm formation of hierarchical scaffolds prepared from a horseradish peroxidase-crosslinking reaction of silk fibroin (SF) combined with zinc (Zn) and strontium (Sr)-doped β-tricalcium phosphate (β-TCP) for OC tissue regeneration. Scaffolds with undoped-β-TCP incorporation were used as control. Results showed that the bilayered scaffolds presented suitable aptitude to support compression and shear loading for OC tissue, with better mechanical properties for the ZnSr-containing structures. Young and shear moduli presented values close to 0.01 MPa in the region 10–20% strain. The investigation of biomaterials surface ability to prevent biofilm formation showed reduced bacterial adhesion of *Escherichia coli* (*E. coli,* gram-negative) and *Staphylococcus aureus* (*S. aureus*, gram-positive) on both scaffolds, thus suggesting that the proposed hierarchical scaffolds have a positive effect in preventing gram-positive and gram-negative bacteria proliferation.

Keywords: silk fibroin, horseradish peroxidase, ZnSr-tricalcium phosphate, hierarchical scaffolds, mechanical strength, antibacterial adhesion, osteochondral regeneration

INTRODUCTION

Irreversible injuries of the hierarchical osteochondral (OC) tissue, triggered by different pathological conditions, can affect both the articular cartilage and the subchondral bone. Currently, autografts or allografts, bone marrow stimulation, cell-based therapy with autologous chondrocytes implantation, and intra-articular injections of mesenchymal stem cells with platelet-rich plasma

(PRP), are the most common surgical methods used for OC tissue treatment (Zhang et al., 2016; Devitt et al., 2017; Bastos et al., 2019). Nevertheless, these treatments are able to reduce pain and cannot warrant the complete regenerative process of the tissue and the articular cartilage healing (De L'Escalopier et al., 2015). Advanced personalized therapies that possibly creating a microenvironment that mimics the OC tissue architecture at the host site may contribute to a faster regeneration (Yousefi et al., 2015). Three-dimensional (3D) scaffolds, with complex, porous and stratified heterogeneous structures, have been renowned as the crucial goal to treat OC damaged tissue, thus serving the mechanical and biological support of the articular cartilage, the subchondral bone and its interface (Drury and Mooney, 2003; Hutmacher, 2006). These structures should hold suitable macro- and micro-porosity, with interconnected and open porosity, thus help cell growth, proliferation, and migration for ECM production (Kang et al., 2018). The degradation and biocompatibility are also imperative attentions for 3D scaffolds manufacturing, assuring their stability, safety, and cost-efficiency (Wang et al., 2008; Ji et al., 2012).

Distinct materials have been emerging as the next generation for scaffolding fabrication, as the case of natural-based polymers (e.g., silk fibroin, collagen, gelatin, chitosan, elastin, fibrin, and albumin), which present superior biocompatibility and low risk of toxicity from the metabolized degradation products (Malafaya et al., 2007; Oliveira and Mano, 2015). Besides, the possibility of combining these biopolymers with inorganic materials [e.g., hydroxyapatite (HAp) and β-tricalcium phosphate (β-TCP)] extend their mechanical performance and osteogenic capacity (Pina et al., 2018). Amongst biopolymers, *Bombyx mori* silk produced by silkworms, as source of silk fibroin (SF) has been attracting great deal of attention in the biomedical field due to its mechanical properties, *in vivo* biocompatibility and biodegradability (Kundu et al., 2013). Furthermore, the hydrophilic and semi-amorphous regions of the SF β-sheet structure can mimic the anionic structure of non-collagenous proteins, acting as deposits of HAp nanoparticles (Marelli et al., 2012). On the other side, β-TCP is one of the calcium phosphate (CaP) compound significantly used as bone grafting substitute material, owed its biocompatibility and resorbability instigating the replacement of implants by the tissues. It is also an adequate ionic carrier, thus playing an essential part in the biological action course, namely enhanced production of bone morphogenetic protein-2 and vascular endothelial growth factors (Bose et al., 2013; Fielding and Bose, 2013). Indeed, many studies have reported the contribution of bioactive inorganic materials functionalized with ionic doping (e.g., strontium, zinc, magnesium, manganese, silicon) to the bone health and to exhibit enhanced biocompatibility and antibacterial properties, while keeping the mechanical properties of the implants (Pina et al., 2010; Mestres et al., 2012). For instance, strontium (Sr) has a bone-seeking behavior encouraging bone formation by osteoblasts, and inhibiting bone resorbtion by osteoclast cells (Saidak and Marie, 2012). Zinc (Zn) has antibacterial properties and is able to stimulate osteoblasts proliferation and differentiation, while stopping the resorption process by osteoclasts (Kandaz et al., 2009). Some works have also reported the use of Sr and Zn as antibacterial agents. Sr-doped HAp exhibited antibacterial activity against *Escherichia coli (E. coli)*, *Staphylococcus aureus (S. aureus)*, and *Lactobacillus* (Lin et al., 2008), and a reduction of bacterial *E. coli*, *S. aureus*, *Candida albicans,* and *Streptococcus mutans* was observed after in contact with HAp incorporating Zn (Chung et al., 2006; Stanić et al., 2010; Thian et al., 2013).

In order to address the OC regeneration challenges, SF combined with ZnSr-doped β-TCP scaffolds has been recently reported (Pina et al., 2017; Ribeiro et al., 2019b). As a first approach, SF were mixed with β-TCP incorporating Sr, Zn, and Mn, to produce biofunctional scaffolds with adequate micro- and macro-porosity for bone tissue regeneration (Pina et al., 2017). *In vitro* assays using human adipose-derived stem cells (hASCs) demonstrated different cellular responses by varying the ionic doping elements in the scaffolds, namely when combined with Sr and Zn in comparison to the single ions. Then, we have proposed a new approach by developing bilayered and hierarchical scaffolds with controlled porosity at the macro- and micro-scale, and improved stability for short- to long-term OC implantation purposes (Ribeiro et al., 2019b). For that, a horseradish peroxidase (HRP)-mediated approach was used to crosslink SF (HRP-SF) combined with ZnSr-doped β-TCP (ZnSrTCP). HRP-SF was used as articular cartilage-like layer, while HRP-SF/ZnSrTCP was used to produce the subchondral bone layer. The scaffolds presented adequate structural integrity, resilient and viscoelastic properties that can be easily adjusted to the OC defect. *In vitro* response of co-cultured human osteoblasts and human chondrocytes indicated osteogenic activity and chondrogenic inducement, respectively in the subchondral and chondral-like layers. The appropriateness of using HRP-crosslinked SF scaffolds was already demonstrated in previous works for cartilage tissue showing the features of enzymatically crosslinked SF hydrogels (Yan et al., 2016; Ribeiro et al., 2018a,b).

In the present study, complementary structural, mechanical properties, and antibacterial activity of the hierarchical scaffolds were investigated. Hence, the failure behavior of the scaffolds was evaluated under combined compression and shear loading, aiming to obtain its strengths for different mode loading conditions. Some concerns with regards to the implant-associated infections, have been reported as one of the most common surgical problems after orthopedic surgeries (Neut et al., 2003; Darouiche, 2004). Therefore, the bacterial adhesion and biofilm formation of the monolayered scaffolds against *E. coli* and *S. aureus* were screened. In particular, it was assessed the antibacterial properties of the scaffolds containing ZnSr as antibacterial agents.

MATERIALS AND METHODS

Preparation of Aqueous SF Solution

Silk fibroin (SF) was extracted from *Bombyx mori* cocoons (Portuguese Association of Parents and Friends of Mentally Disabled Citizens, APPACDM, Castelo Branco, Portugal) by boiling for 1 h in 0.02M sodium carbonate solution (Sigma-Aldrich, St. Louis, MO, United States), to remove the glue-like

sericin protein, and rinsed with distilled water to completely extract the degumming solution. The degummed SF was dissolved in a 9.3M lithium bromide solution (Sigma-Aldrich, St. Louis, MO, United States) for 1 h at 70°C, and dialyzed in distilled water using a benzoylated dialysis tubing (MWCO: 2 kDa) (Sigma-Aldrich, St. Louis, MO, United States) for 48 h. Afterward, the SF solution was concentrated with poly(ethylene) glycol solution (Sigma-Aldrich, St. Louis, MO, United States) to yield a solution of ∼16 wt.%, determined by weighting the dry SF. The SF solution was then stored at 4°C until further use.

Synthesis and Characterization of ZnSr-Doped β-Tricalcium Phosphate (β-TCP) Powders

β-TCP powders doped with 10 mol.% of Sr + Zn (ZnSrTCP) were synthesized using wet chemical precipitation, with a molar ratio of (Ca + Sr + Zn)/P = 1.48, as previously reported (Pina et al., 2017). Calcium nitrate tetrahydrate [$Ca(NO_3).4H_2O$, Sigma-Aldrich, St. Louis, MO, United States], diammonium hydrogen phosphate [$(NH_4)_2HPO_4$, Sigma-Aldrich, St. Louis, MO, United States], strontium nitrate [$Sr(NO_3)$, Sigma-Aldrich, St. Louis, MO, United States] and zinc nitrate [$Zn(NO_3)$, Sigma-Aldrich, St. Louis, MO, United States] were used as starting chemical precursors, respectively for Ca, P, Sr, and Zn. The precipitated suspension was kept for 4 h under constant stirring conditions and ripened for further 20 h under rest conditions, at 50°C and pH ∼7, by adding required amounts of NH_4OH solution. The precipitate was vacuum filtered, dried at 100°C, and heat-treated for 2 h at 1100°C. Then, the powders were ground to fine powders and sieved by a mesh size of 63 μm, showing a final average particle size of 1–10 μm. Pure β-TCP (TCP) powder was also produced for comparison purposes. The crystalline phases presented on the powders were analyzed by X-ray diffraction (XRD) using a conventional Bragg–Brentano diffractometer (Bruker D8 Advance DaVinci, Germany), equipped with CuKα radiation, produced at 40 kV and 40 mA. Data sets were collected in the 2θ range of 10–70° with a step size of 0.02° and 1 s per step. The phase composition of the powders was calculated based on XRD patterns through Rietveld analysis with TOPAS 5.0 software (Bruker, Germany), using the structural model of ICSD card numbers #97500 for β-TCP and #73712 for calcium pyrophosphate ($Ca_2P_2O_7$, β-CPP). Refined parameters were scale factor, sample displacement, background as Chebyshev polynomial of fifth order, crystallite size, and lattice parameters.

Preparation of Hierarchical HRP-Crosslinked SF/ZnSr-Doped β-Tricalcium Phosphate Scaffolds

Hierarchical scaffolds comprising 80/20 (w/w) of HRP-SF/ZnSrTCP as subchondral bone layer and HRP-SF as articular cartilage layer, were fabricated using particulate leaching followed by freeze-drying techniques, as described elsewhere (Ribeiro et al., 2019a,b). Firstly, 1 mL SF (16 wt.%), 50 μL HRP solution (HRP type VI, 0.84 mg/mL) and 65 μL hydrogen peroxide solution (H_2O_2, 0.36 wt.%; Panreac, Barcelona, Spain) (1/0.26‰/1.45‰) was mixed to obtain HRP-SF solution. The subchondral bone-like layer was produced by means of mixing HRP-SF and ZnSrTCP powders. The solution was moved to cylindrical molds (9 mm inner diameter; Deltalab, Barcelona, Spain), and 2 g of granular sodium chloride (low in endotoxins; EMPROVE, VWR BDH Prolabo, Briare, France) with 500-1000 μm (Analytic Sieve Shaker; AS 200 Digit, Retsch, Germany) was added, and left for gelling at 37°C. After that, the molds were immersed in distilled water for salt extraction, for 72 h. The subchondral bone scaffolds were taken out from the molds with a punch (8 mm inner diameter; Smith & Nephew, Portugal). Secondly, HRP-SF solution was placed on the top of the subchondral bone scaffolds, in new silicon molds (8 mm inner diameter) to obtain the articular cartilage-like layer. Then, 2 g of granular sodium chloride (500-1000 μm) was added to the solution and left at 37°C until complete gelation. Then, the bilayered scaffolds were punched (8 mm inner diameter), kept at −80°C and freeze-dried (Telstar Cryodos-80, Barcelona, Spain) for 7 days. Monolayered HRP-SF, HRP-SF/ZnSrTCP, and HRP-SF/TCP scaffolds were also produced for bacteria growth tests. The monolayered scaffolds were denominated as MdTCP and MTCP, respectively for HRP-SF/ZnSrTCP and HRP-SF/TCP scaffolds, while the bilayered scaffolds appear as BdTCP and BTCP, respectively for HRP-SF| HRP-SF/ZnSrTCP and HRP-SF| HRP-SF/TCP scaffolds.

Combined Compression-Shear Properties of the Bilayered Scaffolds

Mechanical testing of the bilayered scaffolds was performed after immersing them in PBS solution (1.37 mM NaCl, 27 mM KCl, 80.6 mM Na_2HPO_4, 19.4 mM KH_2PO_4). Prior to testing samples were stored at 37°C overnight. On the day of testing, samples were blotted dry and their height and diameter were measured three times with repositioning with a digital caliper. Average dimensions were used for subsequent data manipulation. Each sample was secured between two steel compression plates and loaded under simultaneous compression and shear. The loading ramps were synchronized and applied at a rate of 1 mm/min up to a strain of 30% using a custom designed multi-axis testing machine (**Figure 1**) (Holsgrove et al., 2017). Load and displacement data were converted into nominal stress and strain and plotted for each of the five samples tested. Young (E) and shear (G) moduli were evaluated in the region 10–20% strain by fitting experimental data using the least squares technique. Results are presented as mean ± SD.

Antibacterial Properties

Bacterial Cultivation and Inoculums Preparation

Escherichia coli (*E. coli*, gram-negative bacteria; ATCC 25922, US) and *Staphylococcus aureus* (*S. aureus*, gram-positive bacteria; ATCC 25923, US) were used as bacterial models to evaluate the antibacterial performance of the scaffolds. Bacterial cultures were grown in Tryptic Soy broth (TSB) medium, overnight at 37°C incubation. The cultures were centrifuged (9000 rpm), washed in PBS solution and bacteria pellet was then, re-suspended in PBS solution at a concentration adjusted to 1–2 × 10^6 CFU/mL.

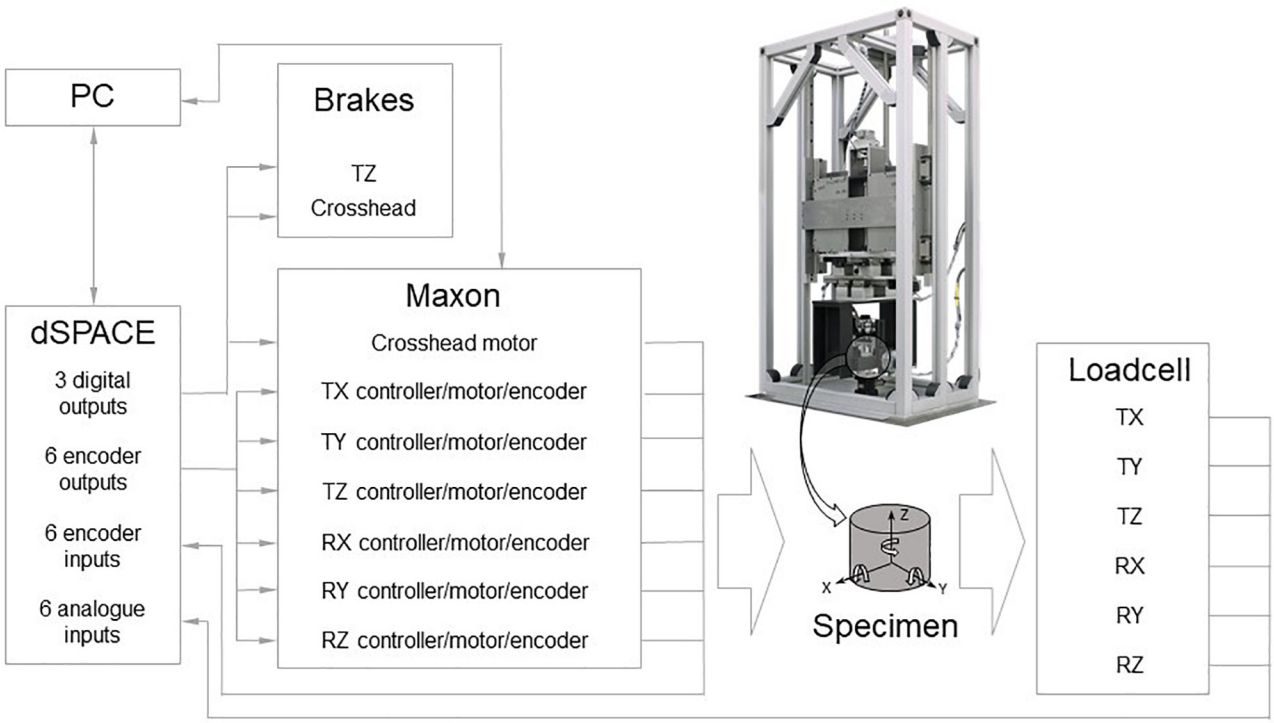

FIGURE 1 | Scheme of the custom designed multi-axis testing machine showing the process for measuring compression and shear stresses simultaneously.

Bacterial Adhesion and Biofilm Formation on the Scaffolds

The *E. coli* and *S. aureus* adherence and biofilm formation on the surface of the portioned HRP-SF, MdTCP, and MTCP scaffolds (8 mm diameter and 3 mm height) were evaluated by seeding the bacteria in a 10 μL suspension of 10^6 CFU/mL on the surface of the scaffolds for 24 h at 37°C incubation. Scaffolds were sterilized by ethylene oxide (Gas Sterilizer/Aerator, Steri-Vac 5XL, 3M Company, Saint Paul, MN, United States). Prior bacteria seeding, all scaffolds were hydrated in PBS solution and keep overnight in the incubator at 37°C.

Bacterial Culture in Liquid Medium

The effects of the HRP-SF, MdTCP and MTCP scaffolds (8 mm diameter and 3 mm height) on *E. coli* and *S. aureus* growth were assessed. Scaffolds were sterilized by ethylene oxide (Gas Sterilizer/Aerator, Steri-Vac 5XL, 3M Company, Saint Paul, MN, United States). First, bacterial liquid cultures were prepared as described above, and then the pre-hydrated scaffolds (incubated overnight at 37°C in PBS solution) were immersed in 1.5 mL of TSB medium containing 10^6 CFU/mL of *E. coli* and *S. aureus*. Scaffolds were incubated with the bacteria for additional 24 h, under agitation. Afterward, the Optical Density (OD; 620 nm) of bacterial suspensions were quantified in a Visible Spectrophotometer (Genesys 30, Thermo Fisher Scientific, Waltham, MA, United States) using gray filters, in order to determine the percentage of bacteria reduction in suspension medium, in the presence of the scaffolds and as a function of the OD in the positive control. Scaffolds without bacterial inoculation were used as negative control, and bacterial cultures without scaffolds were used as positive control. Each experiment was performed in triplicate.

Scanning Electron Microscopy

A high-resolution field emission scanning electron microscope (SEM) with Focused Ion Beam (FIB-SEM; Auriga Compact; Zeiss, Oberkochen, Germany) was used to evaluate bacteria adhesion and the initial formation of biofilm on the scaffolds. The HRP-SF, MdTCP, and MTCP scaffolds recovered after 24 h of direct bacterial seeding and after bacteria culture in liquid medium were first washed with PBS solution and fixed with 2.5% (v/v) glutaraldehyde solution in PBS for 1 h at 4°C in the dark. Afterward, the glutaraldehyde solution was removed, and samples were washed in PBS solution before dehydration in series of ethanol concentrations (30, 50, 70, 90, and 100% v/v). After drying, all samples were platinum sputtered (EM ACE600; Leica, Wetzlar, Germany) and visualized by SEM. Micrographs were taken at an accelerating voltage of 5 kV at different magnifications.

Statistical Analysis

The numerical results are presented as mean ± standard deviation (SD). The GraphPad Prism 5.0 software (GraphPad Software, La Jolla, CA, United States) was used to perform statistical analysis, where a Shapiro–Wilk normality test was first performed to evaluate the data normality. The results indicated

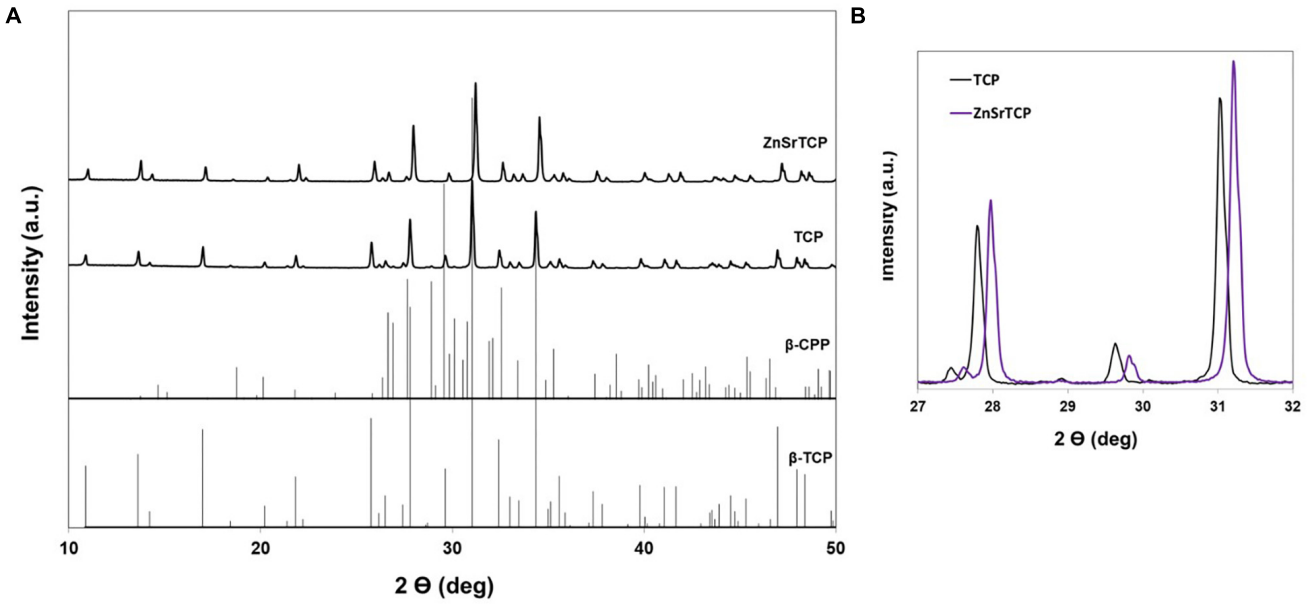

FIGURE 2 | X-ray diffraction patterns of pure TCP and ZnSrTCP powders **(A)**; Zoomed area of **(A)** within the 2θ range from 27 to 32° to show the shift of XRD peaks to higher 2θ angles with ionic incorporation **(B)**. The standard β-TCP (ICDD PDF 04-014-2292) and β-CPP (ICDD PDF 04-009-3876) are also presented for comparison.

that a non-parametric test should be applied for compression-shear mechanical properties results, whereas a parametric test should be used to compare the results of percentage reduction in OD of bacterial suspensions. The results from compression-shear mechanical properties were analyzed by means of a Mann–Whitney test. Five specimens for each composition were tested. A one-way analysis of variance (ANOVA) followed by Tukey's test was used to analyze the percentage reduction in OD of bacterial suspensions. Three independent experiments were performed, using at least two replicates for each condition.

RESULTS

ZnSr-Doped β-TCP Powders

The XRD patterns of pure and ZnSr-doped β-TCP powders are displayed in **Figure 2**. The crystallographic phases were identified based on the standards ICDD PDF 04-014-2292 of β-TCP and 04-009-3876 of β-CPP. It can be seen that the powders consist of β-TCP phase and traces amount of β-CPP, with no amorphous phases. The incorporation of ZnSr into TCP structure is set by a gradual peak shifting (zoomed area **Figure 1B**) of the β-TCP peak to higher angles, thus meaning that the lattice parameters of β-TCP have decreased. The quantitative phase analysis obtained by Rietveld refinement supported the formation of β-TCP as the main crystalline phase with 91 and 9 wt.% of b-CPP in the powders. The refined lattice parameters obtained for standard pure β-TCP were $a = b = 10.439(8)$ Å, $c = 37.395(0)$, $a = \beta = 90°$, and $\gamma = 120°$ in the hexagonal setting (space group R3c) with structural parameters reported by Yashima et al. (2003). These parameters were used as the starting values to refine the data of ZnSrTCP powder. **Table 1** shows a clear decreasing in both lattice parameters along *a*-axis and *c*-axis with ZnSr incorporated, in comparison with TCP powder, thus proving the effective ionic incorporation into β-TCP structure.

Mechanical Properties of the Bilayered Scaffolds

Nominal stress-strain plots for simultaneous axial and shear loading were obtained from load displacement data (**Figure 3**). Young and shear moduli were evaluated for each sample in the region 10–20% strain and then averaged. Neither the Young modulus (0.008 ± 0.006 and 0.009 ± 0.002 MPa for BTCP and BdTCP, respectively) nor the shear one (0.002 ± 0.002 and 0.002 ± 0.001 MPa for BTCP and BdTCP, respectively) showed statistically significant difference when the significance level was set at 0.5. However, a weak tendency of slightly improved mechanical properties was identified for BdTCP scaffolds (**Figure 4**). Besides, the scaffolds were able to preserve their integrity at different loadings.

TABLE 1 | Lattice parameters of β-TCP and β-CPP phases of TCP and ZnSrTCP powders.

	Lattice parameters (Å)			
	β-TCP		β-CPP	
Samples	a	c	a	c
TCP	10.439	37.395	6.690	24.135
ZnSrTCP	10.408	37.302	6.715	23.949

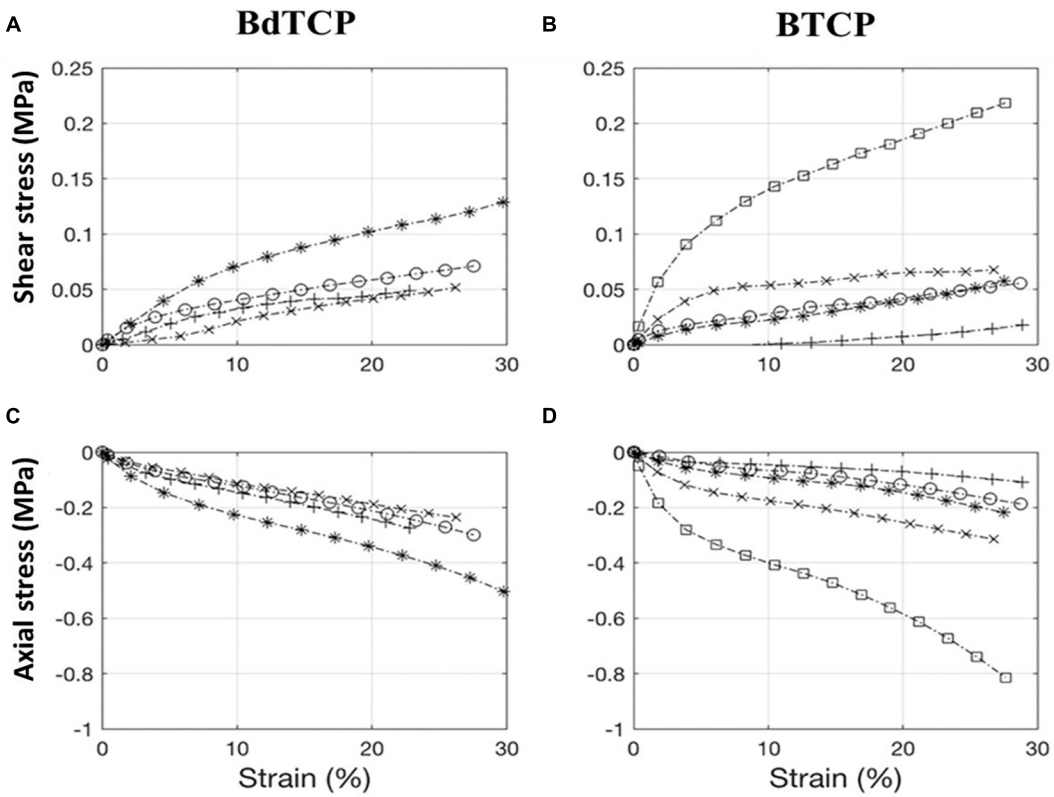

FIGURE 3 | Stress-strain plots for bilayered BTCP and BdTCP scaffolds. Axial compression and shear were applied simultaneously both at a rate of 1 mm/min up to a strain of 30%. BdTCP shear stress and strain **(A)**, BTCP shear stress and strain **(B)**, BdTCP axial stress and strain **(C)**, and BTCP axial stress and strain **(D)**. Results are the mean ± SD of 5 independent experiments. Each curve corresponds to an individual test. The two-curve in **(A–D)** were obtained simultaneously on the same sample, and same symbol refers to the same sample.

Analysis of Bacterial Adherence, Morphology, and Biofilm Formation

SEM Observation After Direct Contact Assay

The adhesion and biofilm formation of *E. coli* and *S. aureus* on the HRP-SF, MdTCP, and MTCP scaffolds was first evaluated by direct contact assay (**Figure 5**). After 24 h of culturing, both bacteria adhered to the HRP-SF scaffolds surface (**Figures 5A,B**) and cross-sections (**Figures 5C,D**), although no biofilm formation was detected. As for the MdTCP (**Figures 5E–H**) and MTCP (**Figures 5I–L**) scaffolds, some poorly distributed bacteria adhered to the scaffolds but at lower levels as compared to the pure HRP-SF scaffolds (**Figures 5A–D**). *E. coli* and *S. aureus* morphology showed cells with regular and smooth shapes and others exhibiting wrinkling, flattening and rupture of the membranes structure. Some cell debris were also detected, which indicates damages of the bacterial walls and loss of cellular content.

Bacterial Viability and Release Profile in Liquid Medium

Bacterial viability in the presence of the HRP-SF, MdTCP, and MTCP scaffolds was evaluated after 24 h of culturing in liquid medium (**Figure 6**). Scaffolds showed no inhibitory effects against *E. coli* growth, presenting a non-significant reduction in OD as compared to the positive control (**Figure 6A**). As for *S. aureus*, a significant reduction (P-value = 0.0098) in OD was detected in the presence of the HRP-SF (72.68 ± 15.14%) and MTCP (73.83 ± 13.71%) scaffolds, in relation to the controls without scaffolds. Even though, both bacteria presented a high viability in the presence of the structures after 24 h of inoculation.

When observed the *E. coli* and *S. aureus* adhesion to the surface of the scaffolds (**Figure 6B**), only a few bacteria were able to adhere while keeping their regular and smooth morphology. Cell debris were observed (red arrows), resulting from the bacterial walls collapse and loss of cellular components. No biofilm formation was observed, and scaffolds were able to maintain their structural integrity during the inoculation period.

DISCUSSION

In the last few years, OC tissue engineering has arisen as an excellent approach to repair and regenerate damaged tissues, avoiding all the limitations of allogenic, autologous, and other available treatments for the tissue healing. Henceforth, 3D scaffolds owing specific structural, mechanical and osteogenic features have been developed addressing articular cartilage

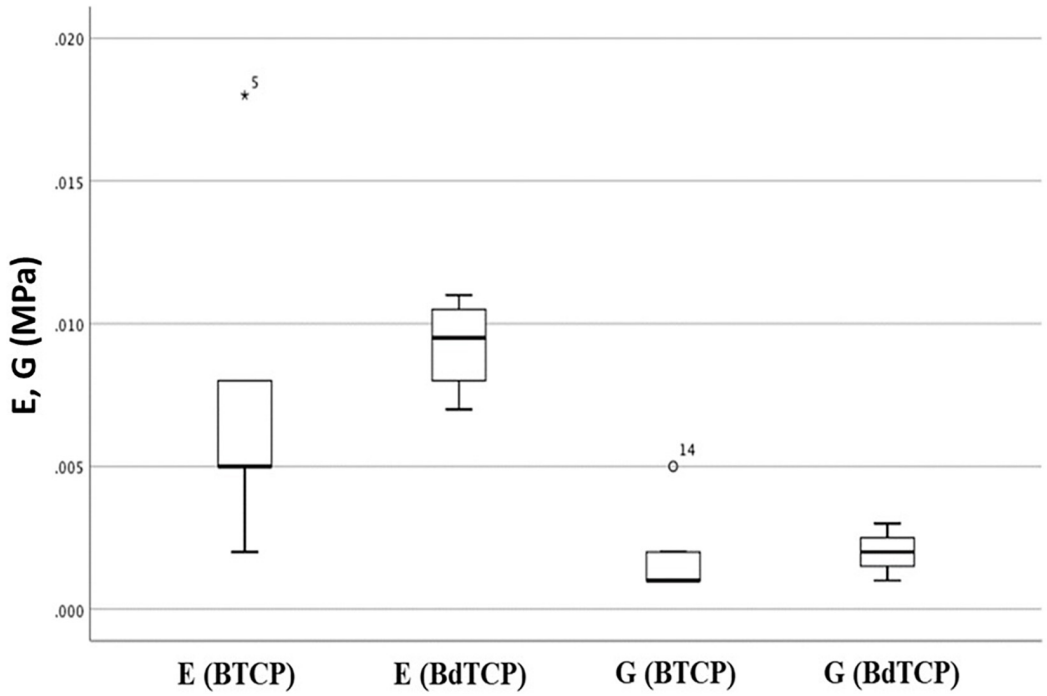

FIGURE 4 | Young (E) and shear (G) moduli for the bilayered pure (BTCP) and doped (BdTCP) scaffolds. Results presented are the mean ± SD of 5 independent experiments.

and subchondral bone regeneration (Drury and Mooney, 2003; Hutmacher, 2006). As aforementioned, our group have recently followed a different approach to produce hierarchically structured scaffolds by using HRP to crosslink SF and to combine it with ZnSr-doped β-TCP nanoparticles as a subchondral bone layer, and HRP-SF as articular cartilage-like layer (Ribeiro et al., 2019b). These scaffolds showed a suitable porous structure with macro-pores larger than 500 μm and micro-pores that reached only 10 μm. The porosity distribution profile showed that in each layer of the hierarchical scaffolds, the pores were evenly distributed, with a mean porosity of 89.1 ± 1.4% in the HRP-SF layer, 31.4 ± 8.4% in the HRP-SF/ZnSrTCP layer and 21.6 ± 8.8% in the HRP-SF/TCP layer. The interface region presented an intermediate porosity of 76.4 ± 2.8 and 71.7 ± 14.6%, respectively in BdTCP and BTCP scaffolds. The scaffolds were able to support human osteoblasts and chondrocytes activity in co-culture conditions, through an extensive cell proliferation profile and ECM production. The *in vivo* response of those scaffolds, after implantation for 8 weeks in rabbit critical size OC defects, exhibited cartilage and calcified tissues repair and regeneration (Ribeiro et al., 2019a). The exceptional assets of using SF namely, the *in vivo* biocompatibility and biodegradability, and excellent mechanical elasticity, illustrate its importance for scaffolds manufacturing (Melke et al., 2016). Particularly, the fibrous structure comparable to collagen type I and type II, brings interest to use SF in orthopedic repair applications (Wang et al., 2006). Furthermore, SF can act as deposition sites of HAp due to its hydrophilic and semi-amorphous sections between the β-sheets, thus mimicking the structure of non-collagenous proteins (Marelli et al., 2012). Different studies have also reported that the crystalline phase of SF may nucleate the deposition of HAp (Vetsch et al., 2015), inducing conformational variations to the protein and presenting superior mechanical properties (Jin et al., 2015). Although SF protein has poor ability for bone regeneration, its blending with inorganic biomaterials by forming a composite material, can improve the final mechanical properties and enhance their osteogenic capacity, thus mimicking the structure of bone tissue. For that reason, the number of publications and annual citations of peer-review original articles related with SF/CaPs composite scaffolds for bone and OC TE applications increased exponentially over the last 20 years, according to the Web of Knowledge database (**Figure 7**). Therefore, joining SF and CaP-based nanopowders result in mechanically stable and osteoconductive scaffolds, thus promoting new OC tissue formation.

In this study, the HRP-SF, pure and HRP-SF/ZnSr-doped β-TCP hierarchical scaffolds were characterized in terms of structural, mechanical and antibacterial properties. Firstly, pure and ZnSr-doped β-TCP were obtained through wet chemical precipitation method, which has the advantage of producing homogeneous powders, and easiness of controlling parameters (i.e., precipitation temperature, and pH) resulting in uniform particles size and morphology, with adequate bioresorbability (Fomin et al., 2008). From XRD patterns and respective refined lattice parameters, the formation of crystalline β-TCP phase and traces of β-CPP on the powders was observed (**Figure 2**). The peak shifts toward higher angles confirmed the successful incorporation of Zn and Sr ions into β-TCP structure. Those

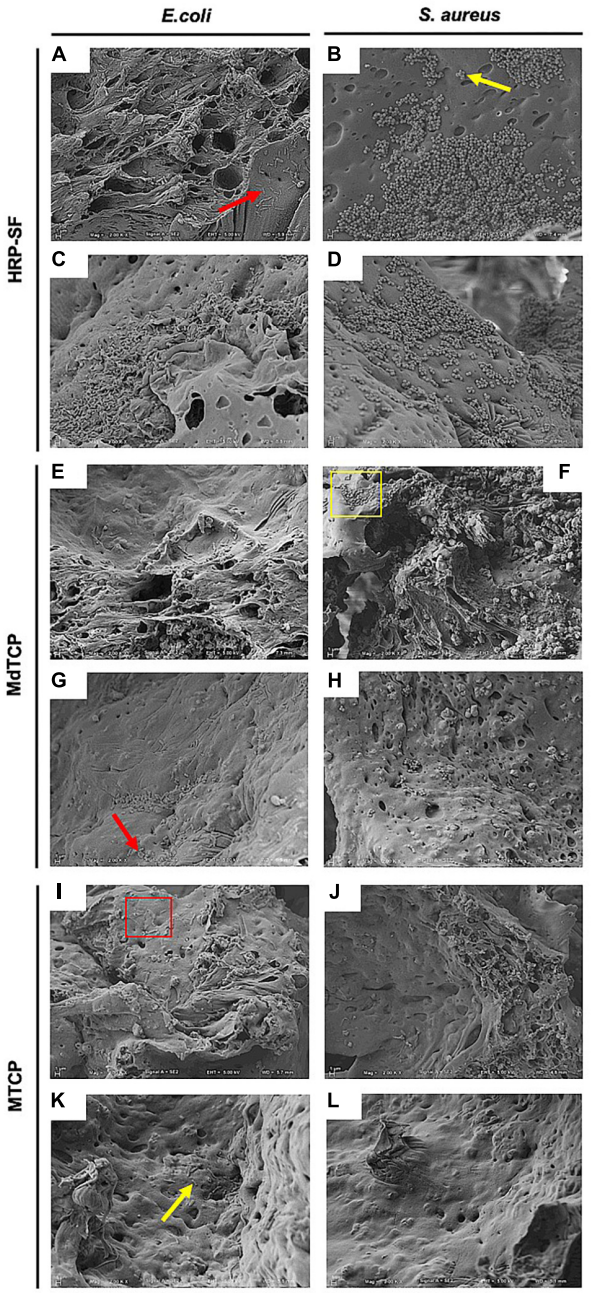

FIGURE 5 | Representative SEM images of *E. coli* and *S. aureus* adhesion and biofilm formation on the **(A–D)** HRP-SF scaffolds, **(E–H)** MdTCP scaffolds, and **(I–L)** MTCP scaffolds after seeding for 24 h. Bacteria adhesion at the **(A,B,E,F,I,J)** surface and **(C,D,G,H,K,L)** cross-sections of the scaffolds. The yellow square and arrows indicate a group of bacteria and individual bacteria with normal surface morphology, respectively. The red square and arrows indicate a group of bacteria or individual bacteria with shape modifications and cell debris, respectively.

changes observed in the lattice parameters unit are ascribed to the ionic radii of Zn (0.74 Å) and Sr (1.12 Å) in comparison to Ca (0.99 Å). Therefore, both *a*-axis and *c*-axis refined lattice parameters increase with higher ionic radii (as Sr), and decrease with smaller (as Zn) ionic radii, than Ca, as reported elsewhere (Kannan et al., 2008, 2009, 2010; Mayer et al., 2008).

Osteochondral lesions are frequently associated with mechanical instability of the joints, thus inducing osteoarthritic degenerative dissimilarities (Martin et al., 2007). Consequently, the mechanical properties of an ideal OC scaffold are of crucial importance, in order to allow the implanted scaffold to bear the physiological loading of the joint without failure or fatigue (Guilak et al., 2001). As previously reported by Ribeiro et al. (2019b), the compressive strengths of BdTCP and BTCP scaffolds were evaluated until a 60% deformation showing respectively, 124.8 ± 23.4 and 92 ± 6.1 kPa. However, considering that human routine activities are subjected to compression, shear and combined compression-shear loading, it is therefore essential the evaluation of the scaffold's strengths, under these combined loadings. Thus, the wet strengths of pure and ZnSr-doped bilayered scaffolds were herein tested under combined compression and shear loading for different mode loading conditions. Results showed Young and shear moduli close to 0.01 MPa, with a tendency of slightly improved mechanical properties for BdTCP, with both keeping their integrity at different mode loading, owing to the binding strength of HRP-SF (**Figures 3**, **4**). The achieved mechanical properties have a small range of values in comparison to the reported ones for natural bone (Young modulus of 1–20 GPa for cortical bone; Young modulus of 10–100 MPa for trabecular bone; shear modulus of 0.2–2 MPa) and for normal human articular cartilage (Young modulus of 0.2–0.3 GPa; shear modulus of 0.1–2 MPa) (Blaker et al., 2005; Sabree et al., 2015). It has been reported that temporary and porous scaffolds may possess compressive modulus of few MPa, which is enough to allow cellularity for ECM mineralization and ingrowth, thus supporting the initial regenerative process (Blaker et al., 2005).

The antibacterial effects and biofilm formation provoked by bacteria adhesion and proliferation on the implants surface may cause acute and chronic infections of the underlying cartilage and bone tissues (Wang et al., 2011). Besides, those effects on biomaterials containing Zn and Sr have been demonstrated on the growth of pathogenic bacteria like *E. coli* and *S. aureus* (Lin et al., 2008; Matsumoto et al., 2009; Wang et al., 2012; Huo et al., 2013). CaPs-based cements and powders have been recognized for having considerable potential for the fully restoration of bone defects in combination with antibacterial properties essential to prevent bacterial infections during implantation procedures (Ewald et al., 2011; Gokcekaya et al., 2017). Although silk sericin has superior antibacterial properties (Karahaliloglu et al., 2017), it has been shown that SF-based materials can be successfully used as supporting matrices for blending with antibacterial polymers in different biomedical applications, including wound dressing (Çalamak et al., 2014, Calamak et al., 2015). Herein, the objective was to evaluate if the monolayered scaffolds are capable of preventing bacterial adhesion to its surfaces and biofilm formation, which is known as a clinical issue involving biomedical devices implantation (O'hara et al., 2018). In fact, alternative biomaterial implants possessing both osteogenic/chondrogenic potential and capable of inhibit

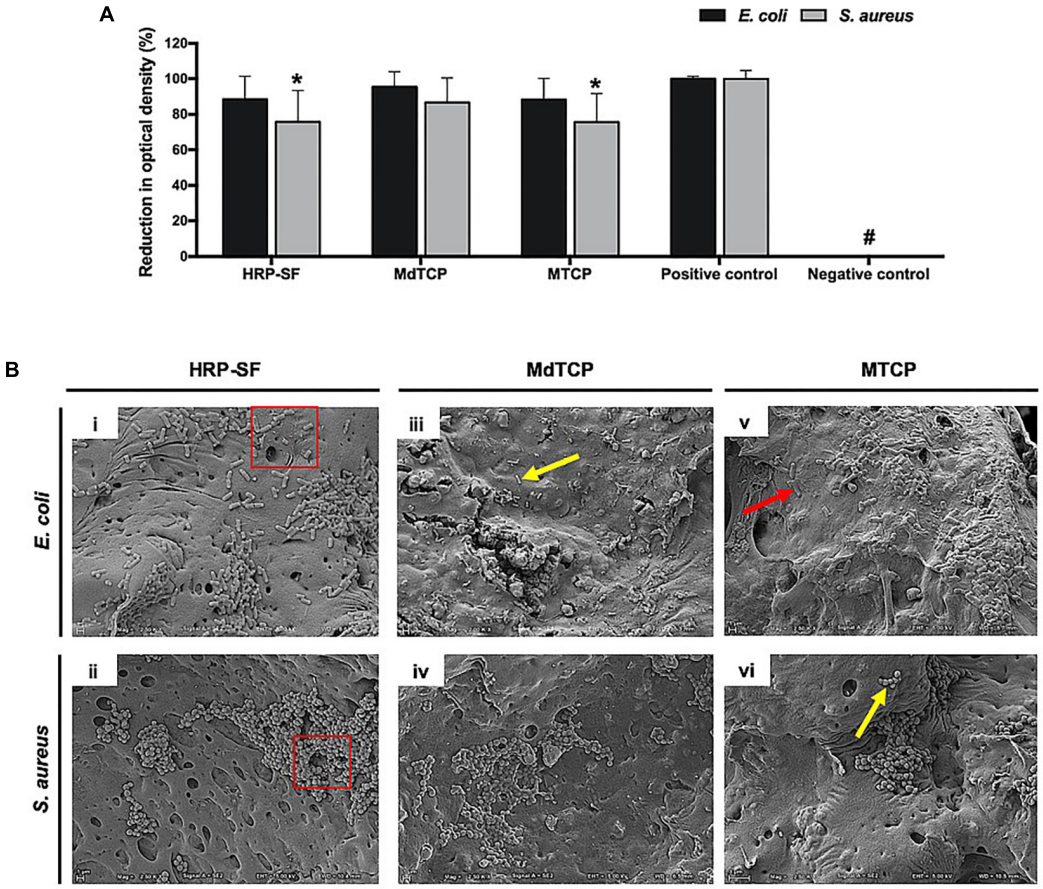

FIGURE 6 | *Escherichia coli* and *S. aureus* cultured in liquid medium, in the presence of HRP-SF, MdTCP, and MTCP scaffolds for the period of 24 h. **(A)** Percentage of bacteria reduction in suspension medium as a function of the OD in the positive control. Data expressed as mean ± standard deviation (SD). *Statistically significant when compared with positive control (*P*-value = 0.0098). HRP-SF (*n* = 7); MdTCP (*n* = 7); MTCP (*n* = 7). # indicate zero-order OD values. **(B)** Representative SEM images of bacteria adhesion and biofilm formation on the (i, ii) HRP-SF scaffolds, (iii, iv) MdTCP scaffolds, and (v, vi) MTCP scaffolds. The yellow arrows indicate normal surface morphology of bacteria. The red squares and arrows indicate a group of bacteria or individual bacteria with shape modifications and cell debris, respectively.

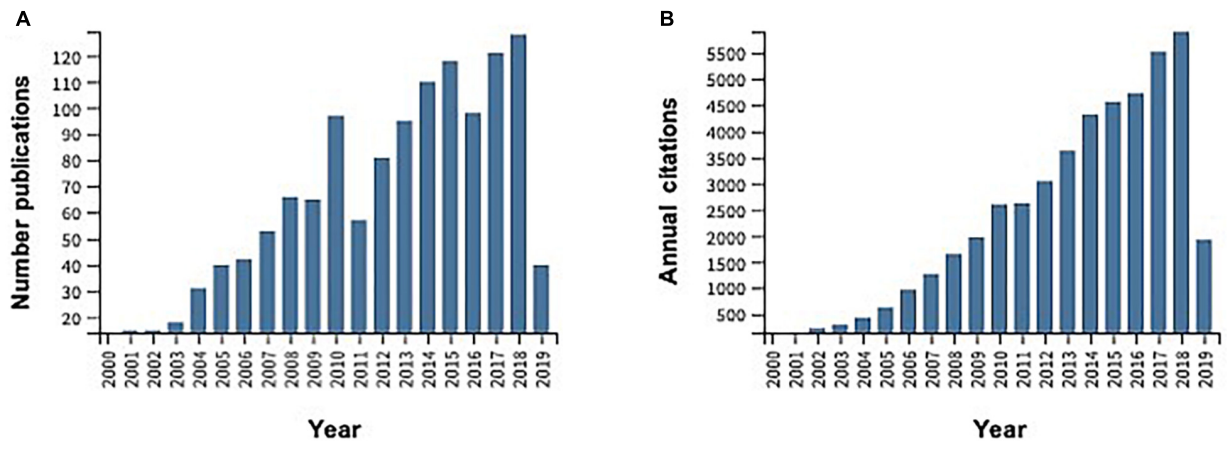

FIGURE 7 | Evolution of the total number of publications per year **(A)** and annual citations **(B)** obtained through a survey in ISI Web of Knowledge under the topic "Silk fibroin and calcium phosphate scaffolds for bone and OC tissue engineering" over the last 20 years.

bacterial colonization have been explored by researchers in the orthopedic community (Zhang et al., 2017; Wang et al., 2019). Although some bacterial adherence was observed in the HRP-SF, MdTCP and MTCP scaffolds after 24 h of cell seeding (**Figure 5**) and culture in liquid medium (**Figure 6B**), all scaffolds were able to prevent biofilm formation of *E. coli* and *S. aureus*. However, the behavior of bacteria adhesion in the cell seeded HRP-SF scaffolds (**Figures 5A–D**) and HRP-SF scaffolds incorporating TCP particles (**Figures 5E–L**) was different. The superior bacterial adhesion observed on the pure HRP-SF scaffolds can be explained by the antibacterial properties of β-TCP (Gokcekaya et al., 2017), and Zn and Sr ions (Lin et al., 2008; Wang et al., 2012), which had a negative effect on *E. coli* and *S. aureus* adherence. Such differences were not observed on the scaffolds cultured in liquid medium, which can be related to the type of bacterial culture used in each assay, namely the different proximity of cells to the scaffolds surface at the time of incubation. Also, the different scaffolds composition had no effects on the adherence of the different bacterial species, despite their distinctive morphologies and cell membranes (Sonohara et al., 1995). However, the shape modifications and cell debris detected in some the adhered bacteria indicate that at some point the proposed scaffolds may play a desired antibacterial effect. Despite the significant reduction in OD of *S. aureus* incubated in the presence of the HRP-SF and MTCP scaffolds (**Figure 6A**), both bacteria presented a high viability (>70% OD) after 24 h of culture in liquid medium and in the presence of the structures (Sonohara et al., 1995). This result can be related to the low release profile from the scaffolds, as shown by the zero-order OD values detected in the controls without bacteria and confirmed that within 24 h no clear biocide effects were induced by the structures despite the bacterial adherence and biofilm formation was prevented. Thus, this can be a valuable approach when hierarchical scaffolds envisioning orthopedic applications are needed, since it can possibly prevent the initial bacterial adhesion to the implanted devices.

CONCLUSION

In this study, the failure behavior under combined compression-shear loading and antibacterial properties of hierarchical scaffolds fully integrating a HRP-SF cartilage-like layer and a HRP-SF/ZnSrTCP subchondral bone-like layer, were assessed. The hierarchical scaffolds presented appropriate ability to support compression and shear loading for OC tissue, with a tendency of improved mechanical properties for the ZnSr-doped scaffolds. The low adherence and absence of biofilm formation on the scaffolds surface using *E. coli* and *S. aureus* have shown that the proposed scaffolds are able to prevent bacterial infections associated with surgical implants. Further studies are necessary to optimize the amount of ZnSr-doped β-TCP on the scaffolds in order to yield more pronounced anti-bacterial effects.

DATA AVAILABILITY STATEMENT

The datasets generated for this study are available on request to the corresponding author.

AUTHOR CONTRIBUTIONS

VR and SP: conceptualization and writing – original draft preparation. VR, SP, AA, and SG: methodology and investigation. SP, SG, RR, and JO: writing – review and editing. JO: supervision. RR and JO: funding administration. All authors agreed to be accountable for the work and to ensure that any questions relating to the accuracy and integrity of the manuscript are investigated and properly resolved.

FUNDING

This research was funded by the Portuguese Foundation for Science and Technology for the Hierarchitech project (M-era-Net/0001/2014), and by the Research and Innovation Staff Exchanges (RISE) action (H2020 Marie Skłodowska-Curie actions) for the BAMOS project (H2020-MSCA-RISE-2016-734156). The authors also thank the funds provided under the distinctions attributed to JO (IF/01285/2015) and SP (CEECIND/03673/2017).

REFERENCES

Bastos, R., Mathias, M., Andrade, R., Amaral, R. J. F. C., Schott, V., Balduino, A., et al. (2019). Intra-articular injection of culture-expanded mesenchymal stem cells with or without addition of platelet-rich plasma is effective in decreasing pain and symptoms in knee osteoarthritis: a controlled, double-blind clinical trial. *Knee Surg. Sports Traumatol. Arthrosc.* doi: 10.1007/s00167-019-05732-8 [Epub ahead of print].

Blaker, J. J., Maquet, V., Jérôme, R., Boccaccini, A. R., and Nazhat, S. N. (2005). Mechanical properties of highly porous PDLLA/Bioglass® composite foams as scaffolds for bone tissue engineering. *Acta Biomater.* 1, 643–652. doi: 10.1016/j.actbio.2005.07.003

Bose, S., Fielding, G., Tarafder, S., and Bandyopadhyay, A. (2013). Trace element doping in calcium phosphate ceramics to understand osteogenesis and angiogenesis. *Trends Biotechnol.* 31, 594–605. doi: 10.1016/j.tibtech.2013.06.005

Calamak, S., Aksoy, E. A., Ertas, N., Erdogdu, C., Sagıroglu, M., and Ulubayram, K. (2015). Ag/silk fibroin nanofibers: effect of fibroin morphology on Ag+ release and antibacterial activity. *Euro. Polym. J.* 67, 99–112. doi: 10.1016/j.eurpolymj.2015.03.068

Çalamak, S., Erdoğdu, C., Özalp, M., and Ulubayram, K. (2014). Silk fibroin based antibacterial bionanotextiles as wound dressing materials. *Mater. Sci. Eng. C Mater. Biol. Appl.* 43, 11–20. doi: 10.1016/j.msec.2014.07.001

Chung, R.-J., Hsieh, M.-F., Huang, C.-W., Perng, L.-H., Wen, H.-W., and Chin, T.-S. (2006). Antimicrobial effects and human gingival biocompatibility of hydroxyapatite sol–gel coatings. *J. Biomed. Mater. Res. B Appl. Biomater.* 76, 169–178. doi: 10.1002/jbm.b.30365

Darouiche, R. O. (2004). Treatment of infections associated with surgical implants. *New Engl. J. Med.* 350, 1422–1429. doi: 10.1056/nejmra035415

De L'Escalopier, N., Barbier, O., Mainard, D., Mayer, J., Ollat, D., and Versier, G. (2015). Outcomes of talar dome osteochondral defect repair using

osteocartilaginous autografts: 37 cases of Mosaicplasty®. *Orthop. Traumatol. Surg. Res.* 101, 97–102. doi: 10.1016/j.otsr.2014.11.006

Devitt, B. M., Bell, S. W., Webster, K. E., Feller, J. A., and Whitehead, T. S. (2017). Surgical treatments of cartilage defects of the knee: systematic review of randomised controlled trials. *Knee* 24, 508–517. doi: 10.1016/j.knee.2016.12.002

Drury, J. L., and Mooney, D. J. (2003). Hydrogels for tissue engineering: scaffold design variables and applications. *Biomaterials* 24, 4337–4351. doi: 10.1016/s0142-9612(03)00340-5

Ewald, A., Hösel, D., Patel, S., Grover, L. M., Barralet, J. E., and Gbureck, U. (2011). Silver-doped calcium phosphate cements with antimicrobial activity. *Acta Biomater.* 7, 4064–4070. doi: 10.1016/j.actbio.2011.06.049

Fielding, G., and Bose, S. (2013). SiO(2) and ZnO Dopants in 3D Printed TCP scaffolds enhances osteogenesis and angiogenesis in vivo. *Acta Biomater.* 9, 9137–9148. doi: 10.1016/j.actbio.2013.07.009

Fomin, A., Barinov, S., Ievlev, V., Smirnov, V., Mikhailov, B., Belonogov, E., et al. (2008). Nanocrystalline hydroxyapatite ceramics produced by low-temperature sintering after high-pressure treatment. *Doklady Chem.* 418, 22–25. doi: 10.1134/s0012500808010084

Gokcekaya, O., Ueda, K., Ogasawara, K., Kanetaka, H., and Narushima, T. (2017). In vitro evaluation of Ag-containing calcium phosphates: effectiveness of Ag-incorporated β-tricalcium phosphate. *Mater. Sci. Eng. C* 75, 926–933. doi: 10.1016/j.msec.2017.02.059

Guilak, F., Butler, D. L., and Goldstein, S. A. (2001). Functional tissue engineering: the role of biomechanics in articular cartilage repair. *Clin. Orthop. Relat. Res.* 391, S295–S305.

Holsgrove, T. P., Miles, A. W., and Gheduzzi, S. (2017). The application of physiological loading using a dynamic, multi-axis spine simulator. *Med. Eng. Phys.* 41, 74–80. doi: 10.1016/j.medengphy.2016.12.004

Huo, K., Zhang, X., Wang, H., Zhao, L., Liu, X., and Chu, P. K. (2013). Osteogenic activity and antibacterial effects on titanium surfaces modified with Zn-incorporated nanotube arrays. *Biomaterials* 34, 3467–3478. doi: 10.1016/j.biomaterials.2013.01.071

Hutmacher, D. W. (2006). "Scaffolds in tissue engineering bone and cartilage," in *The Biomaterials: Silver Jubilee Compendium*, ed. D. F. Williams (Amsterdam: Elsevier).

Ji, W., Yang, F., Seyednejad, H., Chen, Z., Hennink, W. E., Anderson, J. M., et al. (2012). Biocompatibility and degradation characteristics of PLGA-based electrospun nanofibrous scaffolds with nanoapatite incorporation. *Biomaterials* 33, 6604–6614. doi: 10.1016/j.biomaterials.2012.06.018

Jin, Y., Kundu, B., Cai, Y., Kundu, S. C., and Yao, J. (2015). Bio-inspired mineralization of hydroxyapatite in 3D silk fibroin hydrogel for bone tissue engineering. *Colloids Surf. B Biointerfaces* 134, 339–345. doi: 10.1016/j.colsurfb.2015.07.015

Kandaz, M., Ertekin, M. V., Erdemci, B., Kı Zı ltunç, A., Koçer, Í, Özmen, H. K., et al. (2009). The effects of zinc sulfate on the levels of some elements and oxidative stress occurring in lenses of rats exposed to total cranium radiotherapy. *Eurasian J. Med.* 41, 110–115.

Kang, H., Zeng, Y., and Varghese, S. (2018). Functionally graded multilayer scaffolds for in vivo osteochondral tissue engineering. *Acta Biomater.* 78, 365–377. doi: 10.1016/j.actbio.2018.07.039

Kannan, S., Goetz-Neunhoeffer, F., Neubauer, J., and Ferreira, J. M. F. (2008). Ionic substitutions in biphasic hydroxyapatite and beta-tricalcium phosphate mixtures: structural analysis by rietveld refinement. *J. Am. Ceram. Soc.* 91, 1–12. doi: 10.1111/j.1551-2916.2007.02117.x

Kannan, S., Goetz-Neunhoeffer, F., Neubauer, J., and Ferreira, J. M. F. (2009). Synthesis and structure refinement of zinc-doped beta-tricalcium phosphate powders. *J. Am. Ceram. Soc.* 92, 1592–1595. doi: 10.1111/j.1551-2916.2009.03093.x

Kannan, S., Goetz-Neunhoeffer, F., Neubauer, J., Pina, S., Torres, P. M. C., and Ferreira, J. M. F. (2010). Synthesis and structural characterization of strontium- and magnesium-co-substituted β-tricalcium phosphate. *Acta Biomater.* 6, 571–576. doi: 10.1016/j.actbio.2009.08.009

Karahaliloglu, Z., Kilicay, E., and Denkbas, E. B. (2017). Antibacterial chitosan/silk sericin 3D porous scaffolds as a wound dressing material. *Artif. Cells Nanomed. Biotechnol.* 45, 1172–1185. doi: 10.1080/21691401.2016.1203796

Kundu, B., Rajkhowa, R., Kundu, S. C., and Wang, X. (2013). Silk fibroin biomaterials for tissue regenerations. *Adv. Drug Deliv. Rev.* 65, 457–470. doi: 10.1016/j.addr.2012.09.043

Lin, Y., Yang, Z., Cheng, J., and Wang, L. (2008). Synthesis, characterization and antibacterial property of strontium half and totally substituted hydroxyapatite nanoparticles. *J. Wuhan Univ. Technol. Mater. Sci. Ed.* 23, 475–479. doi: 10.1007/s11595-006-4475-2

Malafaya, P. B., Silva, G. A., and Reis, R. L. (2007). Natural–origin polymers as carriers and scaffolds for biomolecules and cell delivery in tissue engineering applications. *Adv. Drug Deliv. Rev.* 59, 207–233. doi: 10.1016/j.addr.2007.03.012

Marelli, B., Ghezzi, C. E., Alessandrino, A., Barralet, J. E., Freddi, G., and Nazhat, S. N. (2012). Silk fibroin derived polypeptide-induced biomineralization of collagen. *Biomaterials* 33, 102–108. doi: 10.1016/j.biomaterials.2011.09.039

Martin, I., Miot, S., Barbero, A., Jakob, M., and Wendt, D. (2007). Osteochondral tissue engineering. *J. Biomech.* 40, 750–765.

Matsumoto, N., Sato, K., Yoshida, K., Hashimoto, K., and Toda, Y. (2009). Preparation and characterization of β-tricalcium phosphate co-doped with monovalent and divalent antibacterial metal ions. *Acta Biomater.* 5, 3157–3164. doi: 10.1016/j.actbio.2009.04.010

Mayer, I., Cuisinier, F. J. G., Gdalya, S., and Popov, I. (2008). Tem study of the morphology of Mn2+-doped calcium hydroxyapatite and β-tricalcium phosphate. *J. Inorg. Biochem.* 102, 311–317. doi: 10.1016/j.jinorgbio.2007.09.004

Melke, J., Midha, S., Ghosh, S., Ito, K., and Hofmann, S. (2016). Silk fibroin as biomaterial for bone tissue engineering. *Acta Biomater.* 31, 1–16. doi: 10.1016/j.actbio.2015.09.005

Mestres, G., Le Van, C., and Ginebra, M.-P. (2012). Silicon-stabilized α-tricalcium phosphate and its use in a calcium phosphate cement: characterization and cell response. *Acta Biomater.* 8, 1169–1179. doi: 10.1016/j.actbio.2011.11.021

Neut, D., Van Horn, J. R., Van Kooten, T. G., Van Der Mei, H. C., and Busscher, H. J. (2003). Detection of biomaterial-associated infections in orthopaedic joint implants. *Clin. Orthop. Relat. Res.* 413, 261–268. doi: 10.1097/01.blo.0000073345.50837.84

O'hara, L. M., Thom, K. A., and Preas, M. A. (2018). Update to the centers for disease control and prevention and the healthcare infection control practices advisory committee guideline for the prevention of surgical site infection (2017): a summary, review, and strategies for implementation. *Am. J. Infect. Control* 46, 602–609. doi: 10.1016/j.ajic.2018.01.018

Oliveira, M. B., and Mano, J. F. (2015). "Natural—based and stimuli—responsive polymers for tissue engineering and regenerative medicine," in *Polymers in Regenerative Medicine: Biomedical Applications from Nano-to Macro-Structures*, eds M. M. Pradas and M. J. Vicent (Hoboken, NJ: John Wiley & Sons, Inc.), 49–90. doi: 10.1002/9781118356692.ch2

Pina, S., Canadas, R., Jiménez, G., Perán, M., Marchal, J., Reis, R., et al. (2017). Biofunctional ionic-doped calcium phosphates: silk fibroin composites for bone tissue engineering scaffolding. *Cells Tissues Organs* 204, 150–163. doi: 10.1159/000469703

Pina, S., Rebelo, R., Correlo, V. M., Oliveira, J. M., and Reis, R. L. (2018). "Bioceramics for osteochondral tissue engineering and regeneration," in *Osteochondral Tissue Engineering: Nanotechnology, Scaffolding-Related Developments and Translation*, eds J. M. Oliveira, S. Pina, J. S. Roman, and R. L. Reis (New York, NY: Springer International Publishing AG), 53–75. doi: 10.1007/978-3-319-76711-6_3

Pina, S., Vieira, S. I., Rego, P., Torres, P. M. C., Goetz-Neunhoeffer, F., Neubauer, J., et al. (2010). Biological responses of brushite-forming Zn- and ZnSr-substituted β-TCP bone cements. *Eur. Cell Mater.* 20, 162–177. doi: 10.22203/ecm.v020a14

Ribeiro, V. P., Da Silva Morais, A., Maia, F. R., Canadas, R. F., Costa, J. B., Oliveira, A. L., et al. (2018a). Combinatory approach for developing silk fibroin scaffolds for cartilage regeneration. *Acta Biomater.* 72, 167–181. doi: 10.1016/j.actbio.2018.03.047

Ribeiro, V. P., Pina, S., Canadas, R. F., Morais, A. D. S., Vilela, C., Vieira, S., et al. (2019a). In vivo performance of hierarchical HRP-crosslinked silk fibroin/β-TCP scaffolds for osteochondral tissue regeneration. *Regen. Med. Front.* 1:e190007. doi: 10.20900/rmf20190007

Ribeiro, V. P., Pina, S., Costa, J. B., Cengiz, I. F., García-Fernández, L., Fernaìndez-Gutieìrrez, M. D. M., et al. (2019b). Enzymatically cross-linked silk fibroin-based hierarchical scaffolds for osteochondral regeneration. *ACS Appl. Mater. Interfaces* 11, 3781–3799. doi: 10.1021/acsami.8b21259

Ribeiro, V. P., Silva-Correia, J., Gonçalves, C., Pina, S., Radhouani, H., Montonen, T., et al. (2018b). Rapidly responsive silk fibroin hydrogels as an artificial matrix for the programmed tumor cells death. *PLoS One* 13:e0194441. doi: 10.1371/journal.pone.0194441

Sabree, I., Gough, J. E., and Derby, B. (2015). Mechanical properties of porous ceramic scaffolds: influence of internal dimensions. *Ceram. Int.* 41, 8425–8432. doi: 10.1016/j.ceramint.2015.03.044

Saidak, Z., and Marie, P. J. (2012). Strontium signaling: molecular mechanisms and therapeutic implications in osteoporosis. *Pharmacol. Ther.* 136, 216–226. doi: 10.1016/j.pharmthera.2012.07.009

Sonohara, R., Muramatsu, N., Ohshima, H., and Kondo, T. (1995). Difference in surface properties between *Escherichia coli* and *Staphylococcus aureus* as revealed by electrophoretic mobility measurements. *Biophys. Chem.* 55, 273–277. doi: 10.1016/0301-4622(95)00004-h

Stanić, V., Dimitrijević, S., Antić-Stanković, J., Mitrić, M., Jokić, B., Plećaš, I. B., et al. (2010). Synthesis, characterization and antimicrobial activity of copper and zinc-doped hydroxyapatite nanopowders. *Appl. Surf. Sci.* 256, 6083–6089. doi: 10.1016/j.apsusc.2010.03.124

Thian, E. S., Konishi, T., Kawanobe, Y., Lim, P. N., Choong, C., Ho, B., et al. (2013). Zinc-substituted hydroxyapatite: a biomaterial with enhanced bioactivity and antibacterial properties. *J. Mater. Sci. Mater. Med.* 24, 437–445. doi: 10.1007/s10856-012-4817-x

Vetsch, J. R., Paulsen, S. J., Müller, R., and Hofmann, S. (2015). Effect of fetal bovine serum on mineralization in silk fibroin scaffolds. *Acta Biomater.* 13, 277–285. doi: 10.1016/j.actbio.2014.11.025

Wang, C., Liu, L.-L., Zhang, A.-T., Xie, P., Lu, J.-J., and Zou, X.-T. (2012). Antibacterial effects of zinc oxide nanoparticles on *Escherichia coli* K88. *Afr. J. Biotechnol.* 11, 10248–10254.

Wang, L., Cao, W., Wang, X., Li, P., Zhou, J., Zhang, G., et al. (2019). Biodegradable silver-loaded polycation modified nanodiamonds/polyurethane scaffold with improved antibacterial and mechanical properties for cartilage tissue repairing. *J. Mater. Sci. Mater. Med.* 30:41. doi: 10.1007/s10856-019-6244-8

Wang, W., Ouyang, Y., and Poh, C. K. (2011). Orthopaedic implant technology: biomaterials from past to future. *Ann. Acad. Med. Singapore* 40, 237–244.

Wang, X., Kim, H. J., Wong, C., Vepari, C., Matsumoto, A., and Kaplan, D. L. (2006). Fibrous proteins and tissue engineering. *Mater. Today* 9, 44–53. doi: 10.1016/s1369-7021(06)71742-4

Wang, Y., Rudym, D. D., Walsh, A., Abrahamsen, L., Kim, H.-J., Kim, H. S., et al. (2008). In vivo degradation of three-dimensional silk fibroin scaffolds. *Biomaterials* 29, 3415–3428. doi: 10.1016/j.biomaterials.2008.05.002

Yan, L.-P., Silva-Correia, J., Ribeiro, V. P., Miranda-Gonçalves, V., Correia, C., Da Silva Morais, A., et al. (2016). Tumor growth suppression induced by biomimetic silk fibroin hydrogels. *Sci. Rep.* 6:31037. doi: 10.1038/srep31037

Yashima, M., Sakai, A., Kamiyama, T., and Hoshikawa, A. (2003). Crystal structure analysis of β-tricalcium phosphate Ca3(Po4)2 by neutron powder diffraction. *J. Solid State Chem.* 175, 272–277. doi: 10.1016/s0022-4596(03)00279-2

Yousefi, A. M., Hoque, M. E., Prasad, R. G., and Uth, N. (2015). Current strategies in multiphasic scaffold design for osteochondral tissue engineering: a review. *J. Biomed. Mater. Res. A* 103, 2460–2481. doi: 10.1002/jbm.a.35356

Zhang, W., Ouyang, H., Dass, C. R., and Xu, J. (2016). Current research on pharmacologic and regenerative therapies for osteoarthritis. *Bone Res.* 4:15040. doi: 10.1038/boneres.2015.40

Zhang, Y., Zhai, D., Xu, M., Yao, Q., Zhu, H., Chang, J., et al. (2017). 3D-printed bioceramic scaffolds with antibacterial and osteogenic activity. *Biofabrication* 9:025037. doi: 10.1088/1758-5090/aa6ed6

Conflict of Interest: The authors declare that the research was conducted in the absence of any commercial or financial relationships that could be construed as a potential conflict of interest.